The critical ventilation velocity in tunnel fires—a computer simulation

C.C. Hwang , J.C. Edwards

National Institute for Occupational Safety and Health, Pittsburgh Research Laboratory, Pittsburgh, PA 15236-0070, USA

Abstract

In ventilated tunnel fires, smoke and hot combustion products may form a layer near the ceiling and flow in the direction opposite to the ventilation stream. The existence of this reverse stratified flow has an important bearing on fire fighting and evacuation of underground mine roadways, tunnels and building corridors. In the present study, conducted by the National Institute for Occupational Safety and Health, a CFD program (fire dynamics simulator) based on large eddy simulations (LES) is used to model floor-level fires in a ventilated tunnel. Specifically, the critical ventilation velocity that is just sufficient to prevent the formation of a reverse stratified layer is simulated for two tunnels of different size. The computer code is verified by checking the computed velocity profile against experimental measurements. The CFD results show the leveling-off of the critical ventilation velocity as the heat release rate surpasses a certain value. At this critical ventilation, the ceiling temperature above the fire reaches a maximum for both tunnels. The velocity leveling-off can be explained from this observation. An extended correlation of Newman (Combust. Flame 57 (1984) 33) is applied to the temperature profiles obtained by CFD. At the critical ventilation, temperature stratification exists downstream from the fire. The computed critical ventilation velocity shows fair agreement with available experimental data taken from both horizontal and inclined fire tunnels. The CFD simulations indicate that the Froude modeling is an approximation for tunnel fires. The Froude-scaling law does not apply to two geometrically similar fire tunnels. The CFD results are compared with two simple theories of critical ventilation by Kennedy et al. (ASHRAE Trans. Res. 102(2) (1996) 40) and Kunsch

Nomenclature

A	tunnel cross-sectional area, m^2
c_p	specific heat, $kJ\,kg^{-1}\,K^{-1}$
Fr	Froude number, dimensionless
g	acceleration of gravity, ms^{-2}
H	tunnel height, m
$\bar{H}$	hydraulic tunnel height, defined as the ratio of 4 times the tunnel cross-sectional area to the tunnel perimeter, m
k	thermal conductivity, $Wm^{-1}\,K^{-1}$
$\dot{m}$	mass flow rate, kgs^{-1}
P	pressure, Pa
$\dot{q}''$	heat flux, Wm^{-2}
Q	chemical heat release rate, kW
Q_c	convective heat release rate, kW
Q^*	dimensionless heat release rate
t	time, s
T	temperature, K
u	ventilation velocity, ms^{-1}
u^*	dimensionless ventilation velocity
V	velocity, ms^{-1}
W	tunnel width, m
x,y,z	Cartesian coordinates, m

Greck letters

ρ	air density, $kg\,m^{-3}$
ϕ	tunnel inclination angle, degree
Ω	a parameter defined in Eq. (9)
ΔT	temperature difference associated with stratification, K
ΔT_0^*	constant with a value equal to 6.13, dimensionless

Subscript

avg	average
b	blackbody
c	convective
cf	difference between ceiling and floor
cr	critical
f	floor
h	temperature rise above ambient near the ceiling
in	tunnel inlet
n	nth band of radiation intensity
O	ambient

ref	reference
s	material

(Fire safety J. 37 (2002) 67).

Keywords: Tunnel Fire; Critical ventilation velocity; Computer simulation; Stratified flow; Froude modeling; Large eddy simulation

1. Introduction

1.1. Critical ventilation velocity

When a fire is started on the floor of a straight tunnel without a ventilation (cross) flow, a hot plume rises above the fire and entrains the surrounding cold air into the plume. The plume, upon reaching the ceiling, forms two gas streams flowing in opposite directions along the ceiling. When a cross ventilation current exists, the symmetry in the rising plume and in the ceiling gas streams is broken. The ventilation current bends the plume and the length of the ceiling layer flowing against the ventilation current is reduced. This situation is depicted in Fig. 1, where the ceiling layer is represented by the gas temperature contours. In Fig. 1, the velocity vectors are also shown to indicate the general flow pattern in the tunnel.

In the event of a tunnel fire or smoke emergency, a main concern is to maintain an evacuation path that is free of smoke and hot gases. The existence of reverse stratified layer (also called back-layer) of hot combustion products has an important bearing on fire fighting and evacuation of underground mine roadways, tunnels and building corridors. Consider a scenario involving a stopped vehicle on fire in a tunnel, disrupting traffic and requiring worker and passenger evacuation. Another scenario involves a conveyer-belt fire in an underground mine entry, producing smoke and toxic combustion products. The consideration

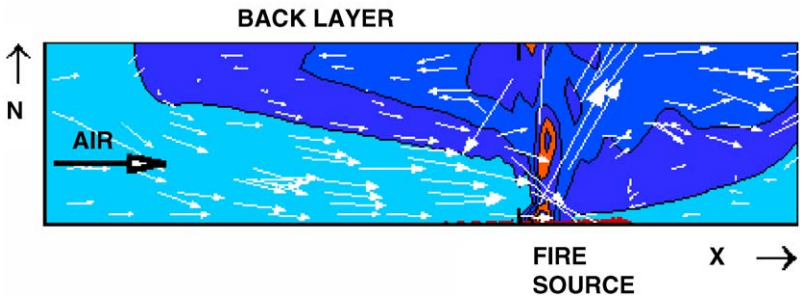

Fig. 1. Stratified ceiling layer of combustion products against the ventilation current from left, with the fire source at the floor.

for emergency planning must focus on determining the ventilation required to maintain a single evacuation path from the fire source clear of smoke and hot gases.

Experimental data show that the length of a back-layer upstream of the fire source is a function of u_{in} for fixed heat release rate from the fire [1–3]. As the value of u_{in} increases, the length of the back-layer decreases. The "critical ventilation velocity" u_{cr} is defined as the value of the ventilation velocity u_{in} that is just able to prevent the formation of a back-layer. In the present CFD study, the ventilation velocity for a given Q is u_{cr} when the front end of the back-layer is at $x = 0$ (front end of the fire source).

The risk from accidental fires as well as the subsequent smoke movement depends largely on this applied ventilation current u_{in}. It is of practical importance to understand the physical parameters and flow conditions under which the reverse stratified flow can be prevented.

1.2. Previous works

Previous authors employed simple empirical models to determine the critical ventilation velocity needed to prevent upstream movement of smoke from a fire in a tunnel [1,4–7]. In general, these models considered the buoyancy head and the dynamic head in the system, and deduced appropriate quantities for correlation. Hwang et al. [8] and Charters et al. [9] employed phenomenological models that provided more detail than the simple empirical approaches. A recent review of tunnel fires by Grant et al. [10] pointed out that existing experimental data still show an inadequate fundamental understanding of the interaction between buoyancy-driven combustion products and forced ventilation, the validity of extrapolation of small-scale results to large scales, the influence of slope on smoke movement, and the effect of tunnel geometry. Wu and Bakar [11] carried out experimental tests of tunnel fires using tunnels of different cross sections. They used the hydraulic diameter as the characteristic length in the dimensionless groups for correlation. The correlation was able to encompass their own data and large tunnel data of other workers. The correlation shows that at large values of Q, u_{cr} levels off. Kunsch [12] derived an expression that shows the decreasing effect of Q on u_{in} as Q increases. His equation shows that the aspect ratio of the tunnel cross-section is also a parameter.

1.3. Objectives of the present study

The present study addresses the problem of critical ventilation velocity in longitudinally ventilated tunnels. Specifically, the leveling-off of u_{cr} for large values of Q is analyzed. Computer simulations are made to see whether the leveling-off of u_{cr} can be observed. If leveling-off of u_{cr} can be simulated, a possible cause is searched and studied. The simulation results are compared with available experimental data and simple theories.

2. Theoretical considerations

2.1. Experimental data

Fig. 2 shows a plot of existing experimental data on the critical ventilation velocity as a function of the heat release rate in fire tunnels. The tunnel size is expressed by the hydraulic tunnel height, $\bar{H}$, defined as $4 \times$ (cross-sectional area)/(perimeter). The values of $\bar{H}$ range from 0.18 to 7.72 m, a factor of 43. Note that the scaling factor $\bar{H}$ is not included in the correlation of Fig. 2. The factor $\bar{H}$ will be included in the correlation in the next section. If we ignore the local variations in the plot, the global trend can be represented by an equation

$$u_{cr} = aQ^{1/5}$$

with u_{cr} in m/s, Q in kW, and α, a constant. An explanation for this 1/5th power correlation will be attempted in Sections after the flow field in the fire plume zone have been studied. If one studies the details of an individual set of experimental data in Fig. 2, especially those of Wu and Bakar [11] and Memorial tunnel [2], one notices the leveling-off of u_{cr} values as Q increases. Other authors also reported this trend

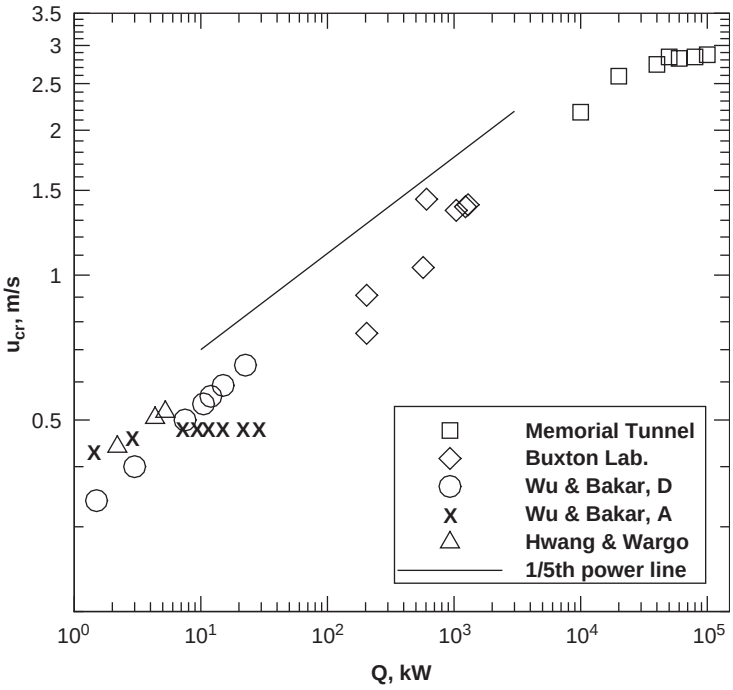

Fig. 2. Experimental data of critical ventilation velocity in tunnel fires. Memorial tunnel: $\bar{H} = 7.72$ m; Buxton lab: $\bar{H} = 2.38$ m; Wu and Bakar, tunnel A: $\bar{H} = 0.176$ m; Wu and Bakar, tunnel D: $\bar{H} = 0.40$ m; Hwang and Wargo: $\bar{H} = 0.343$ m.

[7,10]. A more satisfactory way to treat existing experimental data will be presented in the next Section.

2.2. Scaling parameters

McCaffrey and Quintiere [13] studied buoyancy driven countercurrent flows generated by a fire source, and found that the general nature of the flow is not dependent on scale. This can be achieved by assuming geometric similarity and assuming dynamic similarity holds if the Froude number is maintained constant. The Froude number criterion leads to equal corresponding temperatures between the scaled model (MODEL) and full-scale (FS) systems. The relationship

$$\left(\frac{V}{\sqrt{H}}\right)_{\mathrm{FS}} = \left(\frac{V}{\sqrt{H}}\right)_{\mathrm{MODEL}}$$

holds for velocity V where H is height, provided

$$\left(\frac{Q}{H^{5/2}}\right)_{\mathrm{FS}} = \left(\frac{Q}{H^{5/2}}\right)_{\mathrm{MODEL}},$$

where Q is the heat generated at the fire source. In the correlations of experimental data for tunnel fires, the following dimensionless groups have been used [7,11]

$$u^* = \frac{u_{\mathrm{in}}}{\sqrt{gH}} \quad \text{and} \quad Q^* = \frac{Q}{\rho_0 T_0 c_{\mathrm{p}} \sqrt{gH^5}}. \tag{1}$$

To accommodate for the tunnel cross-sectional geometry, Wu and Bakar [11] used the hydraulic tunnel height $\bar{H}$ in place of H. As shown in Fig. 3, plots of u^*_{cr} versus Q^* encompass the tunnel sizes from 0.18 to 7.7 m. In Fig. 3, a line representing $u^* \propto (Q^*)^{1/3}$ is drawn. This relationship appears to hold for small values of Q^*. The dimensionless critical ventilation velocity u^*_{cr} is defined as the dimensionless value of the ventilation velocity that is just sufficient to prevent the formation of a reverse stratified layer upstream of the fire source. For low values of Q^*, u^*_{cr} increases with Q^*. For high values of Q^*, u^*_{cr} is approximately constant and becomes independent of the value of Q^*. This behavior of the critical-velocity leveling-off has been explained as fire blockage to longitudinal ventilation [7]. Wu and Bakar [11] observed that the temperature distribution in the fire plume changed as the value of Q^* was increased. When the fire heat release rate is increased to certain level, the 'intermittent' flames reach the tunnel ceiling and occupy the upper part of the tunnel. The intermittent flames have the feature of constant flow speed; therefore the buoyancy force in the back-layering is not sensitive to the heat release rate.

2.3. Temperature field in tunnel fires

The previous authors attribute the leveling-off of u_{cr} to fire blocking or intermittent flames. These explanations are related to the flow and temperature fields above and downstream from the fire source. Therefore, a detailed study of the temperature field downstream from the fire may reveal the cause for u_{cr} leveling-off.

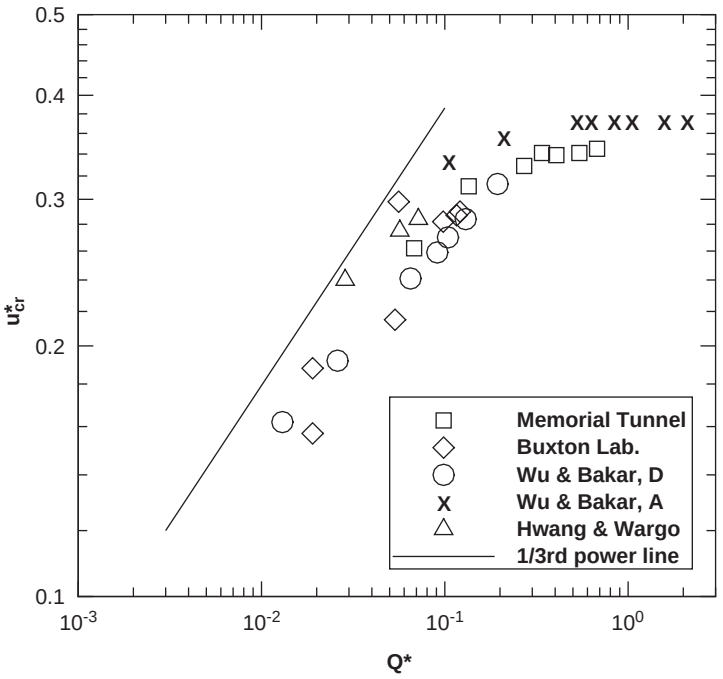

Fig. 3. Experimental data of critical ventilation velocity in tunnel fires using non-dimensional parameters. u^*_{cr} appears to depend on $(Q^*)^{1/3}$ for small values of Q^*.

Newman [14] studied experimentally tunnel fires and expressed his results as shown in Figs. 4 and 5. It is noted that there is a similarity between the line drawn in Fig. 3 and a line connecting points in Fig. 5. In both diagrams, the dependent quantity behaves differently as the independent quantity increases beyond a certain value. This suggests that a quantity associated with the temperature field above the fire may play a role in u_{cr} leveling-off. Our first guess is the temperature stratification under critical ventilation. Newman [14] described the temperature stratification in tunnel fires by

$$\frac{\Delta T}{\Delta T_{ref}} = f(Fr) = f\left\{\frac{V_{ref}}{\left[(\Delta T/T_{ref})g\bar{H}\right]^{1/2}}\right\}, \tag{2}$$

where ΔT is a temperature difference associated with the stratification; T_{ref} is the reference temperature; V_{ref} is the reference flow velocity; g is the acceleration due to gravity; $\bar{H}$ is the characteristic dimension of the duct. The main features of Newman's results (Figs. 4 and 3a in [14]) are shown in Figs. 4 and 5. In Fig. 4, a Froude number is used based on

$$\Delta T = \Delta T_{cf}, T_{ref} = T_{avg}, V_{ref} = V_{avg}$$

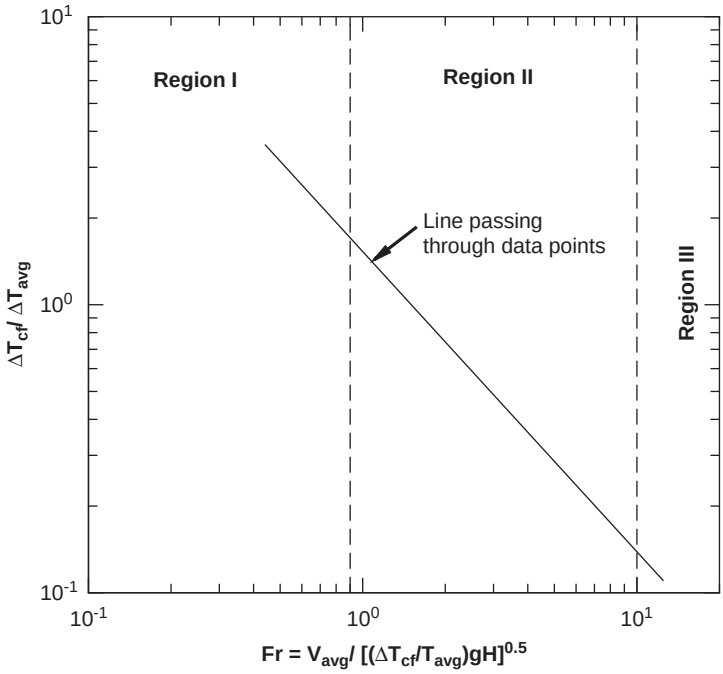

Fig. 4. Gas temperature stratification versus Froude number in tunnel fires. This diagram is based on Fig. 4 of Ref. [14].

where ΔT_{cf} is the difference between the gas temperature near the ceiling and the gas temperature near the floor, and ΔT_{avg} is the average temperature rise relative to ambient. The correlation can be represented by the relationship

$$\frac{\Delta T_{cf}}{\Delta T_{avg}} = 1.5\left\{\frac{V_{avg}}{\left[\left(\Delta T_{cf}/T_{avg}\right)g\bar{H}\right]^{1/2}}\right\}^{-1}. \tag{3}$$

Three regions can be defined in Fig. 4:

Region I: For $Fr \leqslant 0.9, \Delta T_{cf}/\Delta T_{avg} \geqslant 1.7$, i.e., buoyancy dominating temperature stratification.

Region II: For $0.9 \leqslant Fr \leqslant 10$, $1.7 \geqslant \Delta T_{cf}/\Delta T_{avg} \geqslant 0.12$, i.e., significant interaction of the ventilation velocity with the fire-induced buoyancy occurs.

Region III: For $Fr \geqslant 10$, $\Delta T_{cf}/\Delta T_{avg} \leqslant 0.12$, i.e., stratification is insignificant.

Newman [14] also showed (Fig. 5) that for region I, $\Delta T_{cf}/\Delta T_h = 1.0$ independent of $\Delta T_{cf}/\Delta T_{avg}$, where ΔT_h is the gas temperature rise above ambient near the ceiling. This implies that the gas near the floor is essentially at ambient conditions and the maximum temperature stratification is established. In a ventilated tunnel fire, an increase in the heat generation Q increases the temperature stratification that can be

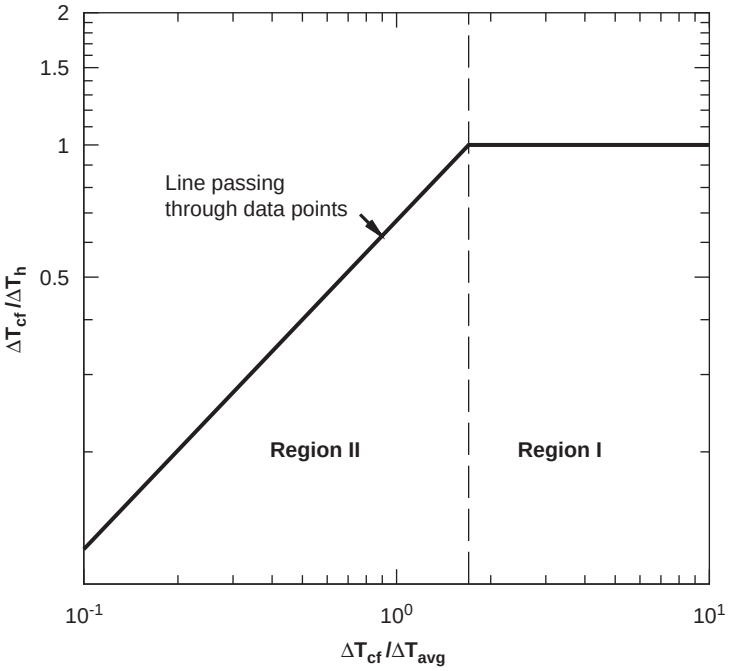

Fig. 5. Gas temperature stratification heptane data in tunnel fires. This diagram is based on Fig. 3a of Ref. [14].

expressed by an increase in the value of $\Delta T_{cf}/\Delta T_h$. Eventually, a condition is reached at which $\Delta T_{cf}/\Delta T_h = 1.0$, and additional increase in Q cannot change the value of $\Delta T_{cf}/\Delta T_h$.

2.4. $u-Q$ relation

When a fire exists in a tunnel of uniform cross-section, the change in the average gas velocity is caused by the change in the gas density. Consider a control volume enclosed by two tunnel cross-sections and the connecting internal walls. The conservation of mass for the control volume gives

$$V_{avg} = \frac{\rho_{in}}{\rho_{avg}} u_{in} \approx \frac{T_{avg}}{T_{in}} u_{in}, \tag{4}$$

where the subscripts "in" designate the condition at the tunnel entrance. Solving for u_{in} from Eqs. (3) and (4) yields

$$u_{in} = 1.5\left(\frac{T_{in}}{T_{avg}}\right)\left(\frac{\Delta T_{avg}}{\Delta T_{cf}}\right)\left[\left(\frac{\Delta T_{cf}}{T_{avg}}\right) g\bar{H}\right]^{1/2} \tag{5}$$

Neglecting changes in the kinetic energy and the potential energy, an energy balance for the control volume gives:

$$Q_c = c_p \dot{m}_{in} \Delta T_{avg} = c_p \rho_{in} u_{in} A \Delta T_{avg} = c_p \rho_{in} u_{in} \frac{\pi}{4} \bar{H}^2 \Delta T_{cf} \frac{\Delta T_{avg}}{\Delta T_{cf}}, \tag{6}$$

where Q_c is the convective heat release rate. It is assumed that the mass addition from the fire source is negligible compared with $\dot{m}_{in}$. Solving for ΔT_{cf} yields

$$\Delta T_{cf} = \left(\frac{\Delta T_{cf}}{\Delta T_{avg}}\right)\left(\frac{4Q_c}{\pi \rho_{in} c_p u_{in} \bar{H}^2}\right). \tag{7}$$

Substituting Eq. (7) into Eq. (5) and solving for u_{in} gives

$$u_{in} = 1.5\left(\frac{4}{\pi}\right)^{1/2}\left(\frac{T_{in}}{T_{avg}}\right)^{3/2}\left(\frac{\Delta T_{avg}}{\Delta T_{cf}}\right)^{1/2}\left(\frac{gQ_c}{\rho_{in} c_p T_{in} u_{in} \bar{H}}\right)^{1/2}. \tag{8}$$

Eq. (8) can be cast into a non-dimensional form

$$\frac{u_{in}}{\sqrt{g\bar{H}}} = 1.42\left(\frac{T_{in}}{T_{avg}}\right)\left(\frac{\Delta T_{avg}}{\Delta T_{cf}}\right)^{1/3}\left(\frac{Q_c}{\rho_{in} c_p T_{in}\sqrt{g\bar{H}^5}}\right)^{1/3}$$

or in terms of the dimensionless group defined by Eq. (1)

$$u^* = 1.42\Omega(Q_c^*)^{1/3} \tag{9}$$

where

$$\Omega = \left(\frac{T_{in}}{T_{avg}}\right)\left(\frac{\Delta T_{avg}}{\Delta T_{cf}}\right)^{1/3}$$

Eq. (9) which relates u^* to Q^* is an extended correlation of Eq. (3). In theory, Eq. (9) applies to a cross-section downstream from a tunnel fire, and should apply to the situation when u^* is the critical ventilation velocity u_{cr}^*. This must be verified in the present simulation. Since the values of T_{in}/T_{avg} and $\Delta T_{avg}/\Delta T_{cf}$ are unknown at this point, a full discussion of Eq. (9) will be delayed until this information is available.

3. CFD simulation

3.1. Turbulence model

In our previous study of the reverse stratified flow generated by a floor-level fire, the standard $k-\varepsilon$ turbulence model was employed for simulation [15]. The advantages of this model are its simplicity and cost effectiveness. For fire applications, one of fundamental limitations of this model is the averaging procedure at the root of the model equations. Since the $k-\varepsilon$ model was developed

as a time-averaged approximation to the conservation equations of fluid dynamics, the results of fire simulations appear smooth. The evolution of eddy structures characteristic of most fire plumes is lost with such an approach [16]. Other known drawbacks of $k-\varepsilon$ model are:

- The model assumes high Reynolds number and has to be adapted for low Reynolds number flows.
- The model assumes an isotropic eddy viscosity and has to be modified to account for the effect of the mean streamline curvature.
- Wall functions (algebraic laws) are generally required to describe flow fields in the vicinity of walls.

Workers dealing with buoyancy-driven flows have used modified versions of the $k-\varepsilon$ model [11,17–19]. The modification in general was made by inclusion of a buoyancy production term in the governing equations. The present study employed a fire dynamics simulator (FDS Version 2) code based on large eddy simulations (LES) techniques [20]. The application of LES techniques to fire is aimed at extracting greater temporal and spatial fidelity from simulation of fire. This model explicitly calculates the turbulent large scales and models the effects of smaller ones using sub grid closure rules. Compared to direct numerical simulations (DNS), the description of the unresolved small scales is lost. Compared to Reynolds ensemble averaging, LES provides the instantaneous resolved field. LES of reacting flows can resolve the instantaneous position of a large-scale flame, so that LES captures the low-frequency variations of flow parameters. The approach based on LES has a particular advantage over the Reynolds-averaging procedures in that only the effects of small-scale turbulence motion have to be modeled [21]. The FDS code adopts the "low Mach number" combustion equations that describe the low speed motion of a gas driven by chemical heat release and buoyancy forces. The balance equations for LES are obtained by filtering the instantaneous balance equations. In the FDS code, the Smagorinsky subgrid-scale model is employed [22]. Although the Smagorinsky model is known as being too dissipative [23], the LES model is believed to be a better model than a $k-\varepsilon$ model for fire simulation. The governing equations for this model can be found in Ref. [16].

3.2. *Combustion model*

The FDS model assumes that the combustion is mixing-controlled and that all species of interest can be described in terms of a mixture fraction [16]. The mixture fraction is a conserved quantity representing the fraction of material at a given point that originated as fuel. The local heat release rate is computed from the local oxygen consumption rate at the flame surface. The flame surface can be located by requiring that fuel and oxidizer simultaneously vanish. The thermal radiation is computed by solving the radiative transport equation (RTE) for a non-scattering gas [16]. In practice, the radiation intensity integrated over a band is solved. Over the wavelength of 1–200 μm, the number of bands is from 6 to 10.

3.3. Description of fire tunnels

In the present study, simulations were performed for two tunnels for which experimental data were available. Fig. 6 shows the schematics of the tunnels with their fire-source geometries. The first (small) tunnel was 4.9-m long with a uniform cross-section 0.4 m wide and 0.3 m high. A fire tunnel of this size was employed to measure distributions of the temperature and velocity in reverse stratified layers generated by floor-level fires [3]. Assigning a volumetric flow rate at the tunnel inlet and atmospheric pressure at the outlet simulated the ventilation flow. In the experiment, natural gas was the fire source burning stoichiometrically at a floor area of 0.15 m axial length and 0.4 m width. In the simulation, methane and propane were used as the fuel. The heat generation per unit area at the fire source (HRRPUA in FDS2) provided the fire intensity for simulation.

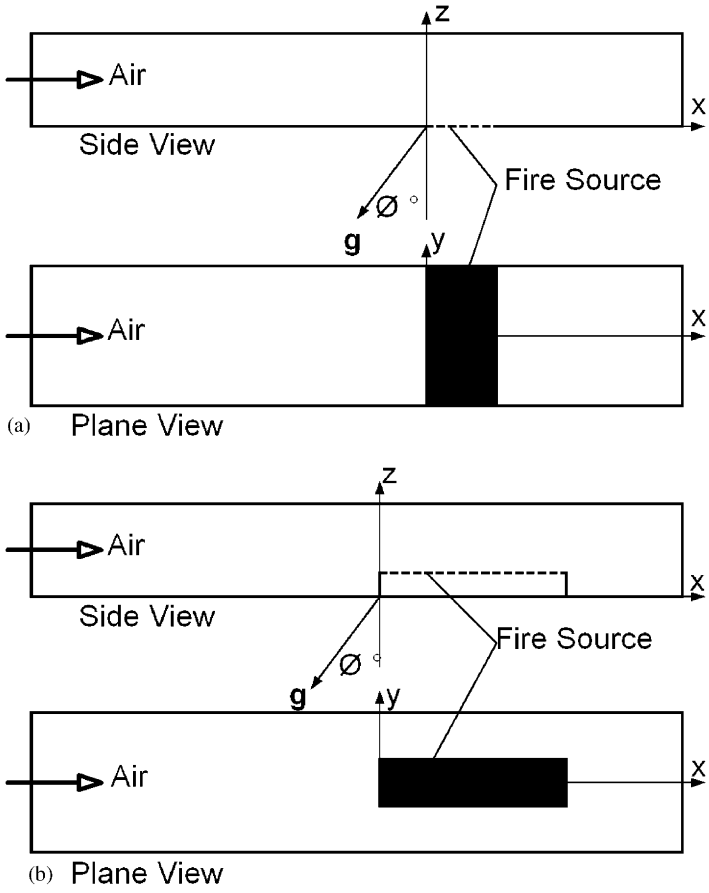

Fig. 6. Schematics of fire tunnels and fire-source configurations. (a) small tunnel; (b) large tunnel. The direction of g (acceleration of gravity) as shown is for ascensional ventilation (uphill slope).

The second (large) tunnel used for simulation was 853 m long, 8.6 m wide and 7.0 m high. The tunnel size was selected to simulate experiments conducted at Memorial tunnel [2]. The tunnel used in the experiments has an arched ceiling. The height of the tunnel for simulation was selected so that the cross-sectional area ($60.2\,m^2$) is equal to that of the experimental tunnel. In the experiments, the fire source was No. 2 fuel oil in various-size pans, with the oil surface at 0.9 m from the floor. In simulation, the fire source was liquid heptane burning stoichiometrically from a plane at a height 1.0 m from the floor. The width of the pan was fixed at 2.6 m wide, so that the length of the pan varied with the total heat generation. For heptane fuel, the heat of vaporization is specified so that the burning rate of fuel is dependent on heat feed back. The data are given in the database of FDS code. Propane was also used in the simulation. For example, the length of the pan for a 50 MW fire is approximately 12 m. In the experiments, jet fans near the tunnel exit provided longitudinal ventilation. In the simulation, a volumetric flow rate was assigned at the exit and atmospheric pressure was assigned at the inlet.

It is seen that the fire-source geometry for these two tunnels are entirely different. The small tunnel has the fire source spread over the entire width of the floor, and the fire intensity is varied by varying the heat generation per unit area. The fire source for the large tunnel, on the other hand, does not occupy the entire width of the floor. It has a fixed heat generation per unit area, and the total fire intensity is linearly proportional to the area of the fire source. This implies that as the fire intensity increases, the longitudinal extent of the fire source increases.

3.4. Boundary conditions

The surface material of the tunnel is assumed thermally thick. A one-dimensional heat conduction equation for the material temperature, $T_s(n,t)$, is applied in the direction $\vec{n}$ pointing into air/solid interface ($n=0$, where n is the normal coordinate)

$$\rho_s c_s \frac{\partial T_s}{\partial t} = k_s \frac{\partial^2 T_s}{\partial n^2}; -k_s \frac{\partial T_s}{\partial n}(0,t) = \dot{q}''_c + \dot{q}''_r$$

where ρ_s, c_s and k_s are the (constant) density, the specific heat and the thermal conductivity of the material; and $\dot{q}''_c$ and $\dot{q}''_r$ are the convective and radiative heat fluxes at the surface [15].

For both tunnels, a uniform velocity is assigned at the inlet and atmospheric pressure is assigned at the exit. In some computations for the large tunnel, atmospheric pressure is assigned at the inlet and volumetric flow rate is assigned at the exit. There was no difference in the computed value of the critical ventilation velocity when the latter boundary conditions were used. At the tunnel wall, the gas velocity has slip as given by the code. This implies that no wall function is used near a wall to accommodate the no-slip boundary condition.

3.5. *Verification of the computer code*

The computer code employed was FDS2 that has been verified in many applications [24–28]. To see how well the code predicts the reverse-stratified flow in a tunnel fire, CFD simulations were made to predict the experimental data of Hwang and Wargo (small tunnel) [3] and the data obtained at the Memorial tunnel (large tunnel) [2]. The descriptions of these tunnels are given in the previous section. The coordinate system (see Fig. 6 for symbols) for the small tunnel was x from –3.05 to 1.85 m, y from –0.2 to 0.2 m, and z from 0 to 0.3 m; the coordinate system for the large tunnel was x from –615 to 238 m, y from −4.3 to 4.3 m, and z from 0 to 7 m. To reduce the computation time, in the computations to determine the critical ventilation velocity, the range of x was −100 m upstream from the fire and 50–90 m downstream from the fire. Compared with the former configuration, it was assumed that the inlet flow development length and an additional length downstream of 50 m had small effect on the results. These assumptions were checked with actual computations. Simulation times up to 300 s were run for both size tunnels. A steady

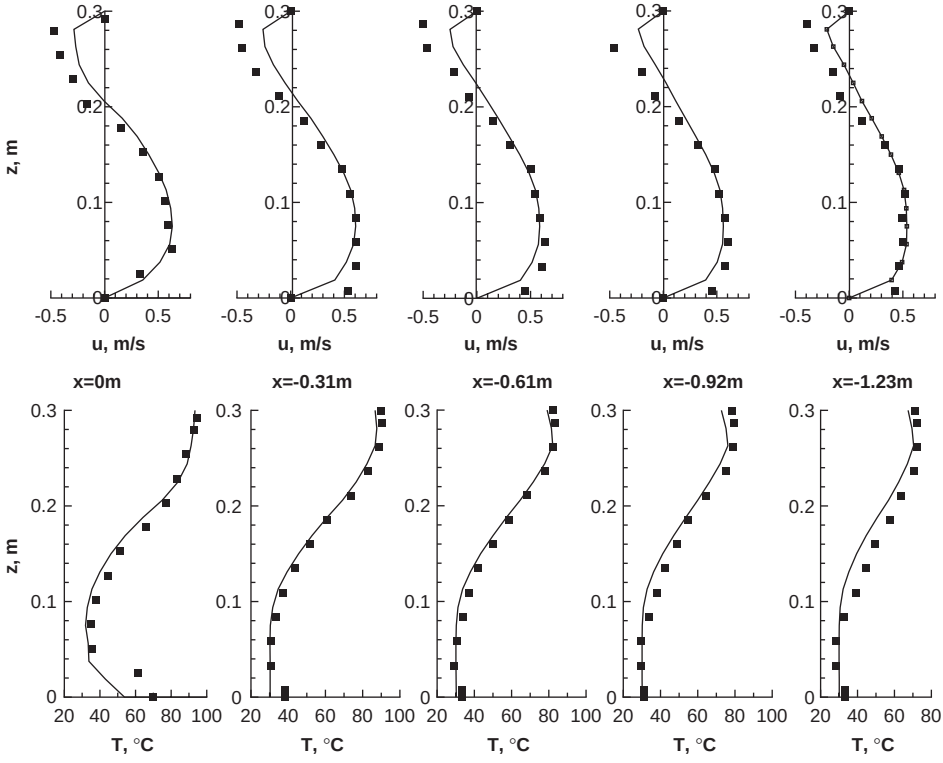

Fig. 7. Comparison of the experimental data (■) of the small tunnel [3] and its prediction (—) by CFD at various cross sections. Upper diagram: velocity profiles. Lower diagram: temperature profiles. Heat generation = 3.3 kW.

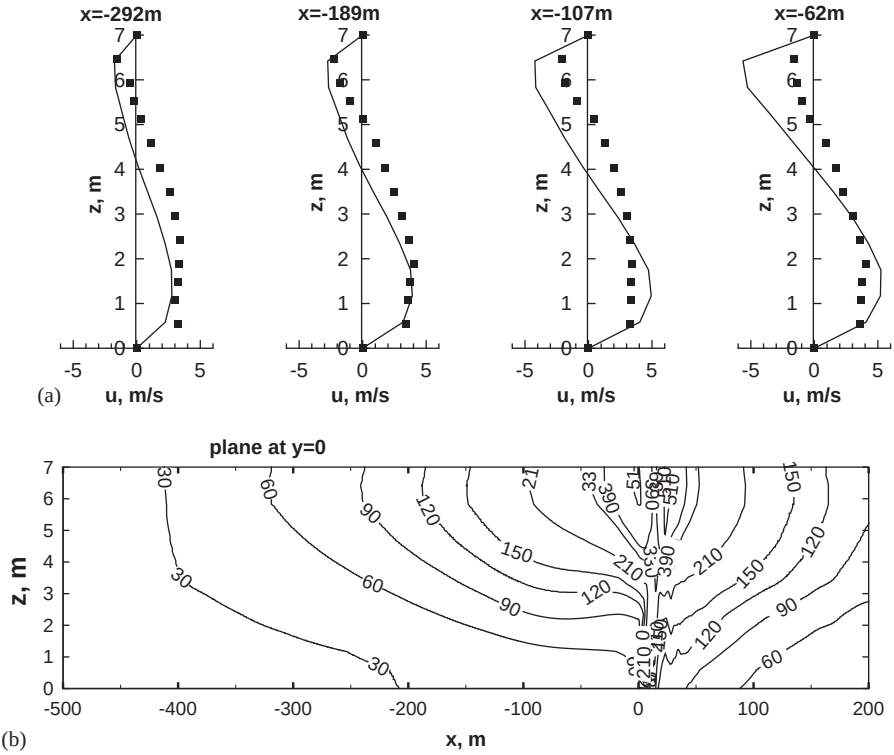

Fig. 8. Results of simulations for the large fire tunnel. (a) Velocity profiles at various cross-section, $y = 0$ plane. Experimental data: ■; CFD prediction: —. (b) Temperature-contour plot in $y = 0$ plane. Heat generation = 50 MW.

state was established by visualizing the layer growth using the 'Smokeview' package in FDS2. Since the measurements were made under steady conditions and an output from LES simulations had flow oscillations, the results from the computations were the mean values from the final 10- to 20-second of the computer outputs.

Fig. 7 shows the velocity and temperature profiles at various stations along the small fire tunnel. Experimental results of Hwang and Wargo [3] are also plotted for comparison. The computations predict the velocity profiles quite well close to the fire zone. In the region upstream of the fire zone, the computations under-predict the ceiling layer velocity and consequently under-predict the layer thickness. Overall, the predicted temperatures agree well with the experiment. Fig. 8 shows the velocity profiles and the temperature contours for the large fire tunnel. The computations over-predict the ceiling layer velocity and the layer thickness. The discrepancy may be attributed to the difference in the configurations of the ceiling region used in the simulation and the actual tunnel. The shape of the temperature contours agrees well with the experimental measurements [2].

Varying the number of grids for both tunnels checked the influence of number of grid cells. For the tunnel having dimensions of $4.9\,\text{m} \times 0.4\,\text{m} \times 0.3\,\text{m}$, two sizes of

Table 1
Effect of cell size for the small tunnel

	Case 1	Case 2
No. of grids	$108 \times 20 \times 16$	$162 \times 36 \times 32$
Cell size	$0.05 \times 0.02 \times 0.0188$ m	$0.033 \times 0.011 \times 0.0094$ m
u_{in} (m/s)	0.620	0.620
Q	10.82 kW	10.73 kW
Layer length (m)	$0.0 < x < 0.200$	$-0.067 < x < 0.233$
Highest temperature at the ceiling (°C)	139 at (0.350, 0, 0.30)	141 at (0.367, 0, 0.30)

Table 2
Effect of cell size for the large tunnel

	Case 1	Case 2
No. of grids	$240 \times 24 \times 24$	$300 \times 30 \times 30$
Cell size	0.3750.3580.292 m	$0.300 \times 0.287 \times 0.233$ m
u_{in} (m/s)	3.17	3.15
Q	16680 kW	17320 kW
Layer length (m)	$-6.38 < x < 9.00$	$-11.1 < x < 9.90$
Highest temperature at the ceiling (°C)	266 at (9.75, 0, 7 m)	256 at (8.70, 0, 7 m)

grids were used. In the first case, the number of grids was $108 \times 20 \times 16$, and in the second case, the number of grids was $162 \times 36 \times 32$. Table 1 shows a comparison of these two cases. The conditions for both cases are close to the critical ventilation conditions as indicated by a short length of the back layering. Both cases have almost identical plots of temperature contours and the velocity vector fields. For the large tunnel, efforts were made to decrease the size of the cells. As a guide, approximately the cell size used by McGrattan et al. [27] in their simulation of a 2 m, 5-MW heptane fire was employed. The cell size for Case 2 (Table 2) was of the order of 0.3 m. The cell size for Case 1 was 25% larger. Because of the scheme with which the heat generation is computed in the code, the value of Q for Case 2 is larger by approximately 4%, and the reverse ceiling-layer length is longer (11.1 versus 6.38 m). Because of slightly different mixing patterns in the fire zone, Case 1 actually has a higher temperature at the ceiling than in Case 2. It is judged that the cell sizes in Tables 1 and 2 are sufficient in the simulation to predict the critical ventilation velocities in tunnel fires. Both cell sizes (Cases 1 and 2) given in Tables 1 and 2 were used in the computations reported in the Results Section.

4. Results

4.1. Critical ventilation velocity, u^*_{cr}

For a fixed heat generation rate Q, the program was run with a selected ventilation velocity (volumetric flow rate) and the formation of the back-flow was checked.

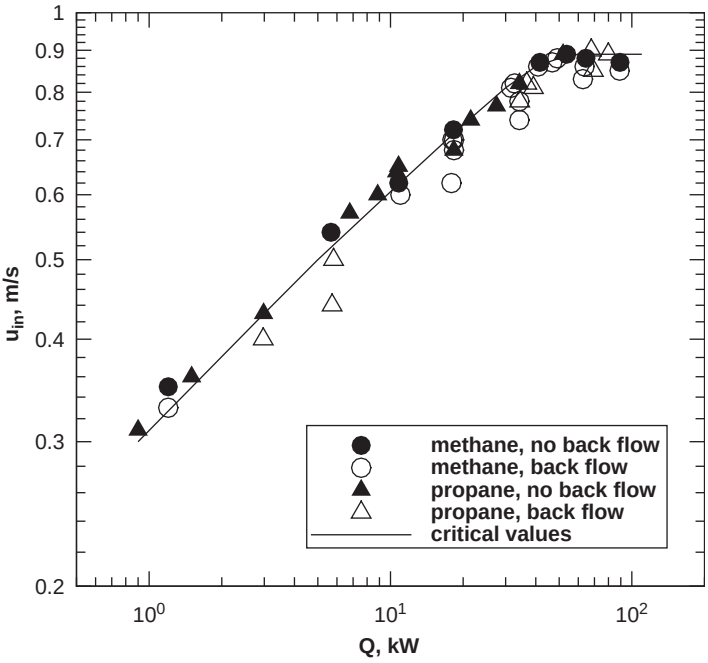

Fig. 9. A diagram used for determination of critical velocities for the small fire tunnel. CFD results. The power of the line at the lower end is 0.299.

Runs were repeated until a range of ventilation velocities encompassed the conditions exhibiting back-flow and no back-flow along the ceiling relative to the upwind edge of the fire zone. Figs. 9 and 10 show the plots of ventilation velocity u_{in} versus the heat generation rate Q for the two tunnels used in the simulation. As shown in Figs. 9 and 10, the demarcation line of the two regions separating back flow and no back flow defines the critical ventilation values. The critical ventilation velocity u_{cr} can then be obtained from these plots as a function of Q. The uncertainty in the values of u_{cr} is $\pm 3\%$ for the large tunnel and $\pm 1.5\%$ for the small tunnel. The uncertainty appears to arise from continuous oscillations in the flow conditions. As mentioned previously, the 'Smokeview' package was employed to study the approach of the steady flow conditions. The relevant flow variables in the last 15–20 s were then averaged for plotting.

The maximum critical velocity is less than approximately 0.9 m/s for the small tunnel and less than approximately 3.5 m/s for the large tunnel. For both tunnels, u_{cr} varies approximately as $Q^{1/3}$ for low values of Q, but u_{cr} levels off for high values of Q. In the small tunnel, methane and propane were used as the fuel. In the large tunnel, propane and heptane were used. Figs. 9 and 10 show that fuel types have negligible effects on the value of u_{cr}. This may be attributed to the computer code which employs the mixture fraction model for combustion, and to the fact that the heat of combustion is approximately same for the hydrocarbon fuels used in the

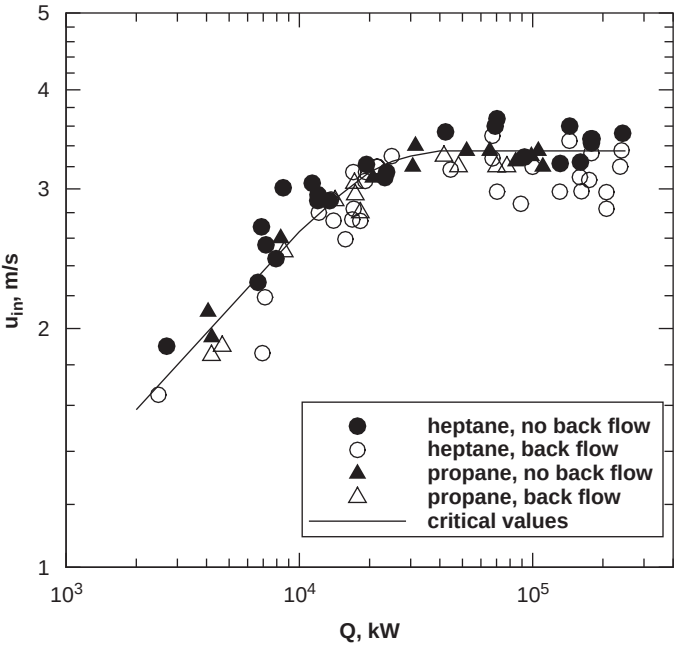

Fig. 10. A diagram used for determination of critical ventilation velocities for the large fire tunnel. CFD results. The power of the line at the lower end is 0.321.

simulation. This suggests that the main parameters affecting u_{cr} are Q and a tunnel dimension H (or $\bar{H}$) as given by Eq (1). Fig. 11 shows non-dimensional plots u^*_{cr} versus Q^* using the values of u_{cr} versus Q obtained from Figs. 9 and 10. As seen in Fig. 11, the scaling parameters introduced to non-dimensionalize the plots collapsed the data from two different size tunnels into curves sitting side by side. If the scaling were perfect, the two curves would merge into one. It is noted that in Froude modeling, the Reynolds number (viscous force) is ignored and the radiation and conduction groups may not be preserved. At high heat generation rates, i.e., $Q^* \geqslant 0.3$, the value of u^*_{cr} is approximately independent of Q^*. Other workers have observed this trend [7,11]. Fig. 11 also shows experimental data from small-scale tunnels [11] and large-scale tunnels (given in [11]) that are included in Fig. 2.

4.2. *Froude modeling*

As observed in Fig. 11, various experimental data and CFD results cannot be collapsed into a single curve by applying the scaling parameter $\bar{H}$. This indicates that the Froude modeling is only an approximation for these data sets. This is expected because there is no geometric and dynamic similarity among these data sets.

To assess the effects of tunnel size and fire-source geometry on the Froude modeling, a series of CFD runs are performed. Tunnels I(a) and I(b) in Table 3 are geometrically similar with a scale factor of 21.5. The width of tunnel I(a) is equal to

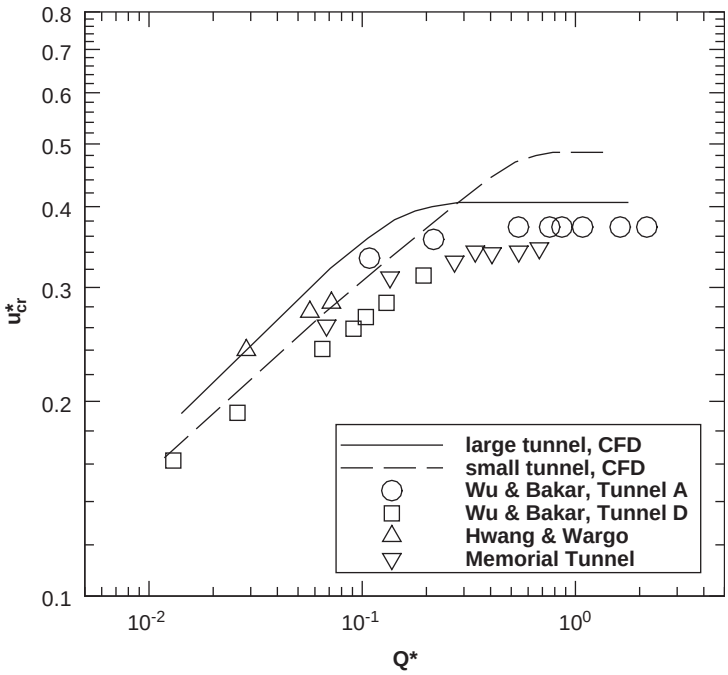

Fig. 11. Non-dimensional plots of the critical ventilation velocity versus the fire heat generation, showing a comparison of CFD and experimental results.

Table 3
The effects of tunnel size and fire-source geometry on the Froude modeling

Case		$\bar{H}(m)$	Q(kW)	u_{cr}(m/s)	Q^*	u^*_{cr}	Fire source (m)	Fuel	Remarks
I	(a)	0.343	11.1	0.605	0.145	0.330	0.15×0.4	CH_4	[a]
	(b)	7.37	24,000	3.41	0.147	0.401	3.23×8.6	CH_4	[a]
	(c)	0.343	11.6	0.66	0.152	0.360	0.5×0.12	CH_4	
II	(a)	0.343	4.7	0.463	0.062	0.252	0.15×0.4	CH_4	[a]
	(b)	0.686	26.6	0.71	0.062	0.274	0.30×0.8	CH_4	[a]
	(c)	0.343	4.8	0.51	0.063	0.278	0.5×0.12	CH_4	
III	(a)	7.72	15,100	3.04	0.082	0.349	9.92×2.6	C_3H_8	
	(b)	7.72	15,400	2.79	0.084	0.321	3.0×8.6	C_3H_8	[a]
IV	(a)	7.72	44,800	3.60	0.244	0.414	10.8×2.6	C_7H_{16}	
	(b)	7.72	46,300	3.96	0.252	0.455	3.3×8.6	C_7H_{16}	[a]
V	(a)	0.343	119	0.875	1.557	0.477	0.15×0.4	CH_4	[a]
	(b)	0.343	121	0.99	1.584	0.540	0.5×0.12	CH_4	

[a]Fire source spans across the tunnel floor.

that of the small tunnel and the width of tunnel I(b) is equal to that of the large tunnel. The tunnel length of I(b) is smaller than that of the large tunnel used in the computation. The values of Q^* are adjusted to be approximately equal for Cases I(a)

and I(b). The value of u_{cr}^* for I(b) is 21% larger than that for I(a). This observation alone may account for the separation of the lines for the CFD results in Fig. 11. Cases I(a) and I(c) compare the effect of the fire-source geometry on u_{cr}^*. Case I(a) has a fire source spanning across the cross-section, while Case I(c) has a rectangular fire source along the axis of the tunnel. Both fire-source areas are equal. The value of Q^* for Case I(c) is 5% greater than that of Case I(a), the value of u_{cr}^* is 9% greater. Case II is similar to Case I with different value of Q and different ratio of the tunnel size. The trends are similar. Case III and IV show the effects of the fire-source geometry on the value of u_{cr}^*. The effects are opposite depending on the value of Q. The fuel type is shown to have a negligible effect on u_{cr}^*, the effect appears to be the fire-source geometry or other effect such as radiation which is not considered in the Froude Modeling. In Case V, very high values of Q are considered. The effect of fire-source geometry is similar to that observed in Cases I and II.

In a geometrically similar tunnel, altering the fire-source geometry alters the kinematics of flow. Dynamical similarity can no longer be preserved. Fig. 12 are vector plots showing the velocity fields along a cross-sectional plane for Cases I(a) and I(c) in Table 3. Fig. 12(a) has the fire source spanning across the floor, showing upward flows along the entire floor. The upward flow is bent over at about 1/3rd of the tunnel height by the ventilation flow. The ventilation-flow vector is approximately perpendicular to the cross-sectional plane, and cannot be represented in Fig. 12. Fig. 12(b) has the fire source running the center region of the floor, producing a rising fire plume in the center region of the cross-section. The vector plots in a cross-sectional plane at $x = 2.15\,\mathrm{m}$ for Case I(b) (not shown) also show upward flow along the entire floor, but bends over at about 1/6th of the tunnel height. At the upper corners, strong streams toward the center region are visible. There is no such stream in Fig. 12(a). Case I(a) and I(b) are geometrically similar tunnels, yet the flow patterns are different at the geometrically similar locations. These CFD simulations confirm that the Froude-scaling law expressed by the parameters in Eq. (1) is an approximation for tunnel fires.

4.3. *Effects of tunnel inclination on* u_{cr}^*

For the same fire-source conditions, the critical ventilation velocity is dependent on channel inclination angles. Fig. 6 shows that when the tunnel inclination angle is positive ($\phi > 0$), the ventilation flow is ascensional. Experiments show that a tunnel with rising air-flow ($\phi > 0$, uphill slope) requires a smaller critical ventilation velocity than that with horizontal air-flow [3]. Fig. 13 shows the results of the present CFD and the experimental data of Hwang and Wargo [3] both with $Q = 4.5\,\mathrm{kW}$. The CFD results are in good agreement with the experimental results. Also shown are CFD results for $Q = 35\mathrm{kW}$. It may be noted that the $u_{cr} - \phi$ relationship is non-linear.

Atkinson and Wu obtained experimentally expressions for the critical velocity in tunnels that slope downhill with an angle between 0° and 10° [29]. The expressions

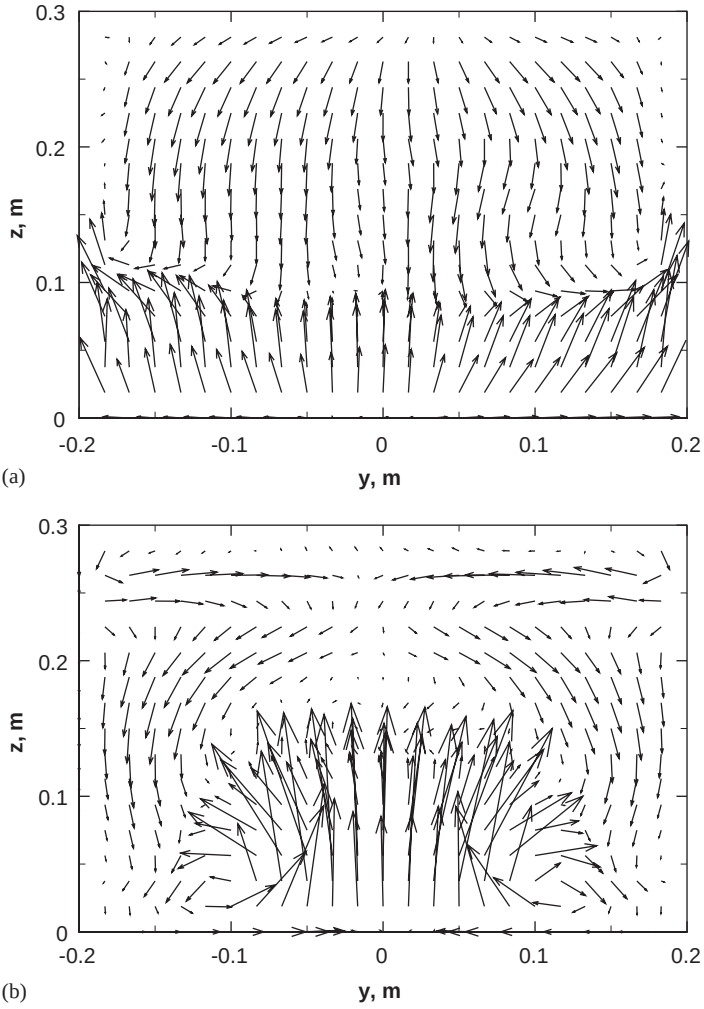

Fig. 12. Vector plots of the flow fields downstream of the fire source. (a) Case I(a) in Table 3 with $Q = 11.1\,\mathrm{kW}$ and $u_{cr} = 0.605\,\mathrm{m/s}$. Tunnel cross-section at $x = 0.1\,\mathrm{m}$ (inside of fire source). (b) Case I(c) with $Q = 11.6\,\mathrm{MW}$ and $u_{cr} = 0.66\,\mathrm{m/s}$. Tunnel cross-section at $x = 0.1\,\mathrm{m}$ (inside of fire source).

show that the critical velocity u_{cr} varies linearly with the inclination angle ϕ:

$$u_{cr} = (g\bar{H})^{1/2} u^*_{max} \left(\frac{Q^*}{0.12}\right)^{1/3} (1 - 0.014\phi) \text{ for } Q^* < 0.12, \tag{10}$$

$$u_{cr} = (g\bar{H})^{1/2} u^*_{max} (1 - 0.014\phi) \text{ for } Q^* > 0.12 \tag{11}$$

It is noted that ϕ is negative for a downhill slope. (Note that Eq. (5) of their paper has an error). Their results are also shown in Fig. 13. For $Q^* < 0.12$ (corresponding to $Q = 4.5\,\mathrm{kW}$), Eq. (10) checks well with the results of Hwang and Wargo [3]. For

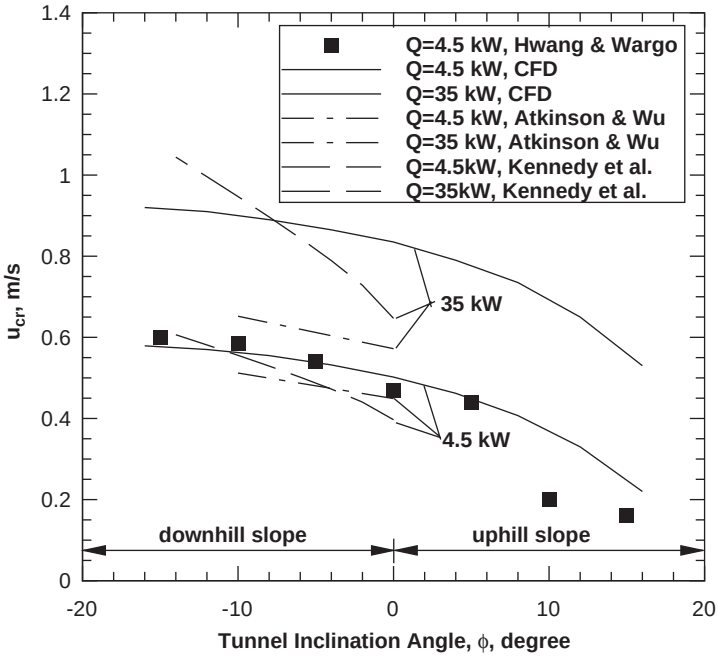

Fig. 13. Effects of channel inclination on the critical ventilation velocity. Positive inclination angle corresponds to ascensional ventilation air-flow.

$Q^* > 0.12$ (corresponding to $Q = 35\,\mathrm{kW}$), Eq. (11) under-predicts the results of the present computation.

Kennedy et al. [6] have an expression for the effect of tunnel inclination that is a part of the equations for computing u_{cr}:

$$u_{cr} = K_1 K_g \left[\frac{gHQ}{\rho c_p A T_f}\right]^{1/3} \tag{12}$$

with

$$K_1 = Fr_{cr}^{-1/3},$$

$$K_g = 1 + 0.0374(grade)^{0.8}$$

$$T_f = \frac{Q}{\rho c_p A u_{cr}} + T_{in}$$

where A is the tunnel cross-sectional area, Fr_{cr} is the critical Froude number, taken as 4.5, "grade" is the absolute value of the tunnel downgrade in %, and T_{in} is absolute temperature of approaching air. Eq. (12) is employed to predict u_{cr} for the small tunnel with downgrades from 0° to 10°. The results are shown in Fig. 13.

Table 4
Effect of ambient temperature on the critical ventilation velocity

Temperature (°C)	Q(kW)	u_{in}(m/s)	Layer length (m)	
			Min. x	Max. x
5	4.53	0.50	−0.08	0.32
15	4.54	0.50	−0.04	0.28
25	4.52	0.50	−0.08	0.28
35	4.52	0.50	−0.04	0.32

Eq. (12) slightly under-predicts the experimental results. The factor representing the effect of tunnel inclination K_g appears to over-predict the effect.

4.4. *Effects of ambient temperature on* u^*_{cr}

A series of runs were made to see any effect of the ambient temperature on the critical ventilation velocity. The ambient temperature was varied from 5 to 35 °C for given values of Q and u_{in}. Table 4 shows the results of this study using the small tunnel. As the ambient temperature was varied, the ceiling-layer position and its layer length stayed approximately unchanged. This implies that within the variation of the ambient temperature studied, the ambient temperature has negligible effect on the critical ventilation velocity.

4.5. *Temperature maximum at critical ventilation*

The trend that the critical ventilation velocity u^*_{cr} is approximately independent of the fire heat generation Q^* beyond approximately $Q^* \approx 0.3$ will be discussed. The present CFD simulation found that as Q was increased maintaining the critical-ventilation conditions, the temperature field at the ceiling region above the fire source approached a maximum. Fig. 14 shows the temperature contours at $y = 0$ plane for the small tunnel under the critical ventilation conditions. Referring to Fig. 9, the three values of Q's selected represent the values at 1/3rd-power region of the line, at the transitional region, and at the constant-u_{cr} region. In Fig. 14(a), with a low value of Q the temperature at the ceiling region is low at approximately 40 °C. In Fig. 14(b), Q is increased to 53 kW, and the ceiling temperature is now 100–350 °C. As Q is increased to 89 kW in Fig. 14(c), the ceiling temperature stays at approximately 200–350 °C. In Fig. 15, the temperature contours at $y = 0$ plane are for the large tunnel. In reference to Fig. 10, the three values of Q selected represent those at 1/3rd-power region of the line, at the transitional region, and at the constant-u_{cr}. The ceiling temperatures in Figs. 15(a)–(c) are approximately 100, 200–250, and 200–250 °C, respectively. It may be noted that, despite a difference in the tunnel size and the heat release rate, the temperatures above the fire source as shown in Fig. 14(b), (c) and 15(b), (c) do not exceed about 350 °C. At the critical ventilation, the back layering terminates at $x = 0$ and the fire plume tilts forward. In

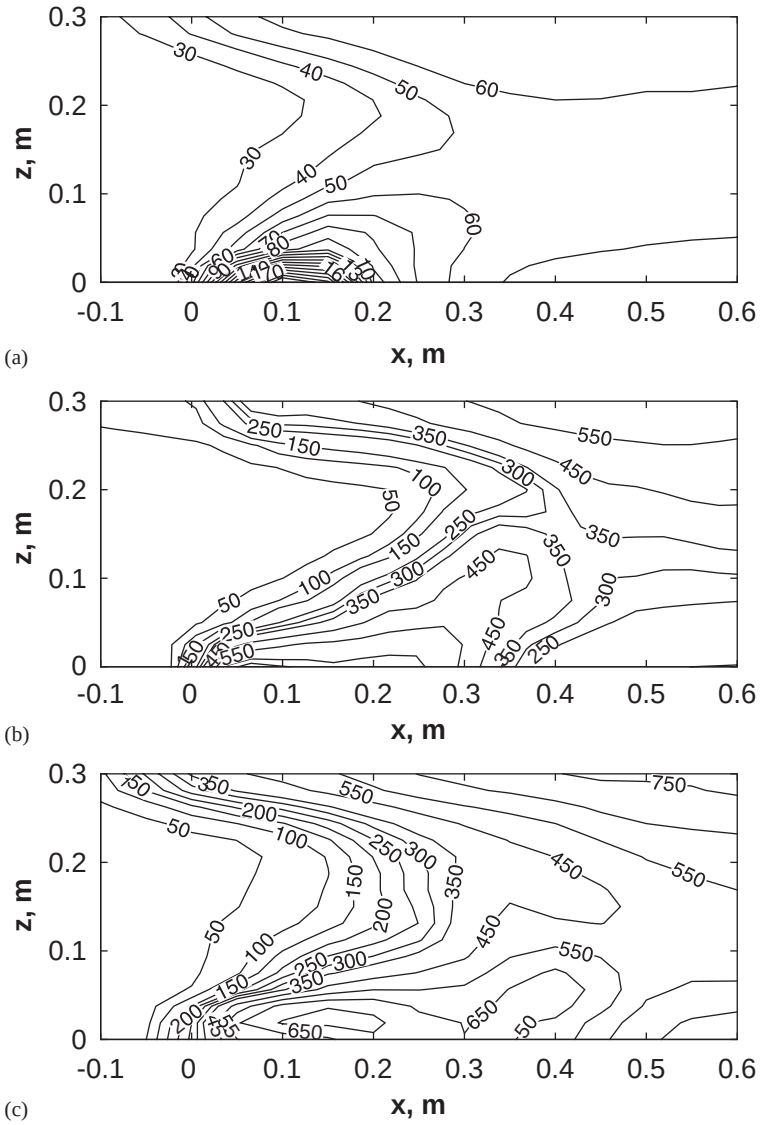

Fig. 14. Temperature contour at $y = 0$ plane for the small tunnel, showing the conditions at the critical ventilation. (a) 3 kW; (b) 53 kW; (c) 89 kW.

a ventilated tunnel, the forward layer carries more heat energy than the back layer. At low Q's, to maintain the back layer at $x = 0$, u_{cr} increases as Q increases. As Q increases close to a value for which u_{cr} levels off, the fire plume bends to the extent that the back layer receives the same amount of heat energy. Any additional heat energy goes to the forward layer. At this point, u_{cr} is unchanged and sustains the back layer at $x = 0$, even though Q keeps increasing. For Figs. 14(b), (c) and 15(b),

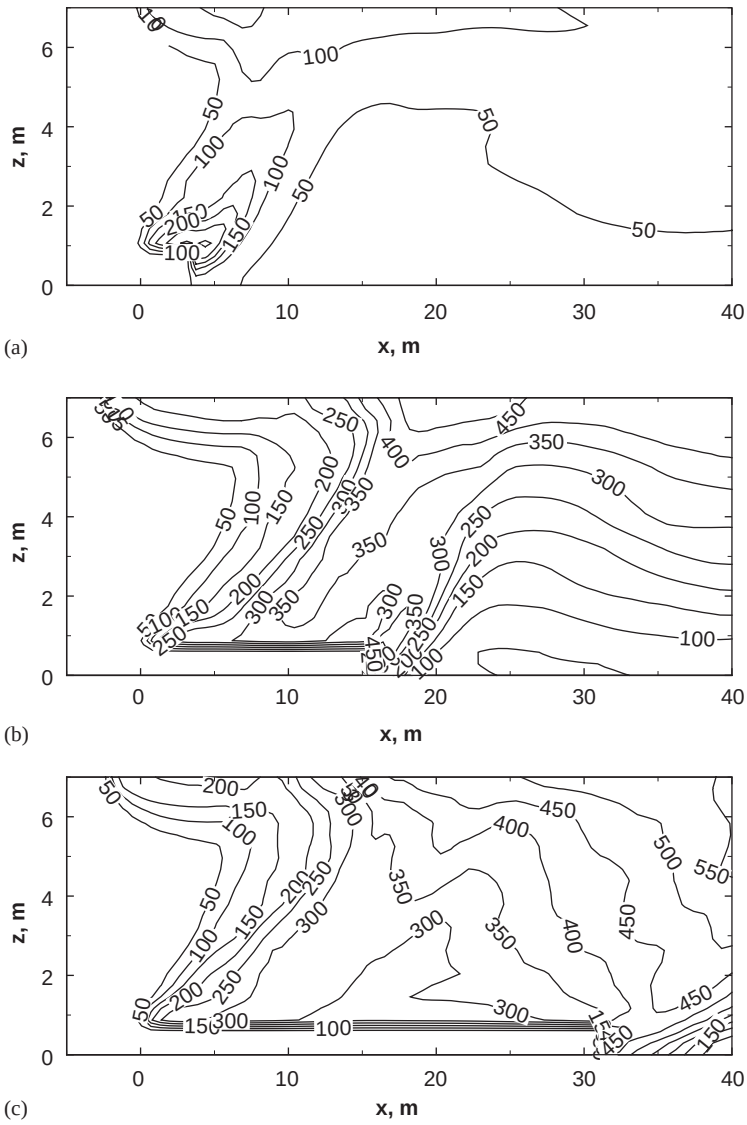

Fig. 15. Temperature contours at $y = 0$ plane for the large tunnel, showing the conditions at the critical ventilation. (a) $Q = 13$ MW; (b) $Q = 67$ MW; (c) $Q = 144$ MW.

15(c) the maximum temperature is reached for critical ventilation. The attainment of a temperature maximum at the critical ventilation provides a demarcation at which u_{cr} no longer changes as Q increases. It may be noted from Figs. 14 and 15 that the forward-layer temperature may reach much higher level than the maximum temperature.

4.6. Temperature stratification

An analysis of Eq. (9) requires temperature profiles downstream from the fire. Because of a large variation in a given cross-section in the region downstream from the fire source, the temperature profile at a cross-section is obtained by averaging in the y-direction for a given value of z. The value of T_{avg} for a cross-section A is computed by the equation

$$T_{\text{avg}} = \int \frac{\rho u T \, \mathrm{d}A}{\rho u \, \mathrm{d}A}$$

Fig. 16 shows the temperature profiles for the cases shown in Figs. 14 and 15. The cases (a)B, (a)C (small tunnel) and (b)B, (b)C (large tunnel) correspond to the leveling-off of u^*_{cr} in Fig. 11. As shown in Table 5, the estimated u^*_{cr} agrees well with the CFD value except for Case (a)A in which Eq (9) over-estimates the CFD value. Except in Case (a)A, there is a range of x-values at which the temperature profiles yield u^*_{cr} approximately equals to the CFD vlalue.

The parameter used by Newman [14] for temperature stratification $\Delta T_{\text{cf}}/\Delta T_{\text{avg}}$ is not consistent for Case (b)A. A more appropriate parameter appears to be the ratio $\Delta T_{\text{cf}}/T_{\text{avg}}$. By comparing the values in Table 5 with the temperature profiles in Fig. 16, the degree of temperature stratification is consistent with the value of $\Delta T_{\text{cf}}/T_{\text{avg}}$. It appears that when this value reaches approximately 0.75 in critical ventilation, the temperature stratification is complete, and leveling-off of u^*_{cr} takes place. It is noted that the value of 0.75 applies to both the small and the large tunnels.

Based on the forgoing analysis, Eq. (9) is shown to predict the relationship of $u^*_{\text{cr}} - Q^*$ in Fig. 11. In summary, the following statement may be made for Eq. (9):

$$\text{As } Q^* (\text{or } Q^*_c) \to 0, \quad \frac{T_{\text{in}}}{T_{\text{avg}}} \to 1 \text{ and } \frac{\Delta T_{\text{avg}}}{\Delta T_{\text{cf}}} \to \frac{0}{0}, \text{ indeterminate.}$$

But the right-hand side of Eq. (9) becomes u^*_{cr} as $Q^* \to 0$, so that $\Delta T_{\text{avg}}/\Delta T_{\text{cf}}$ is a large constant. Therefore,

$$\Omega \to \text{const. as } Q^* \to 0,$$

and

$$Q^* \to \text{large values}, \Omega \propto (Q^*)^{-1/3}.$$

The last statement is difficult to argue; however, the CFD values for u^*_{cr} in Table 5 appear to verify the statement.

4.7. Explanation using a free plume

Oka and Atkinson [7] tried to explain the observed trend using results for a free plume [30]. This argument is presented in the following. For a very small fire where

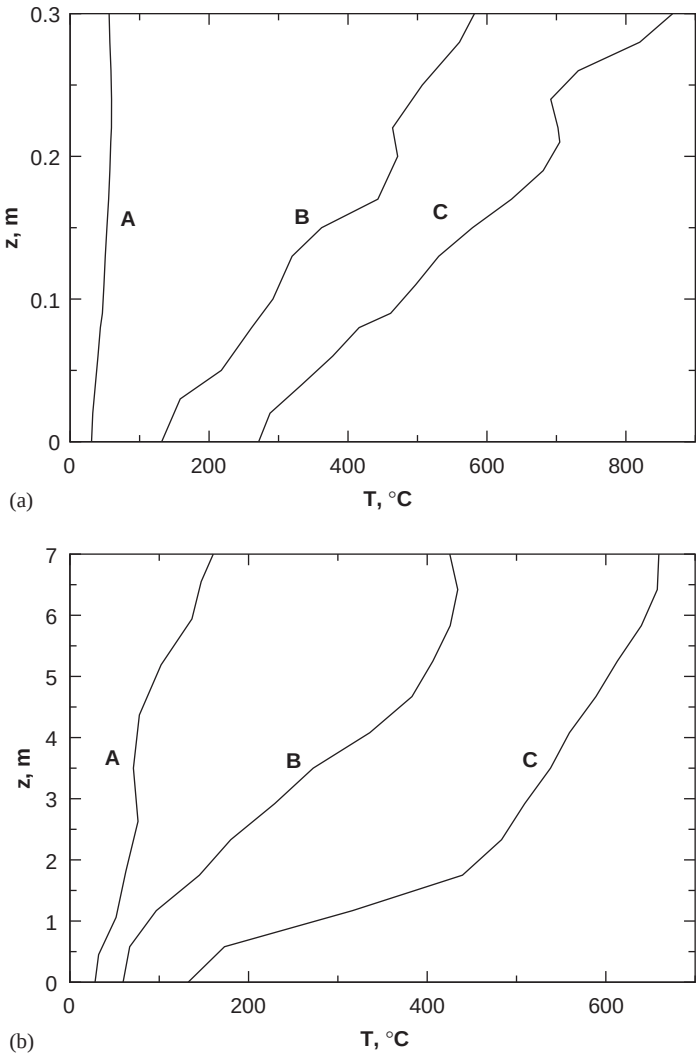

Fig. 16. Temperature profiles downstream of the fire source. (a) Small tunnel: Profile A $\Rightarrow$ Fig. 14(a), $x = 1.85$ m; Profile B $\Rightarrow$ Fig. 14(b), $x = 0.61$ m; Profile C $\Rightarrow$ Fig. 14(c), $x = 1.05$ m. (b) Large tunnel: Profile A $\Rightarrow$ Fig. 15(a), $x = 10$ m; Profile B $\Rightarrow$ Fig. 15(b), $x = 37$ m; Profile C $\Rightarrow$ Fig. 15(c), $x = 51$ m.

the flame length is a small fraction of the tunnel height,

$$\Delta\rho \propto \frac{Q^{2/3}}{z^{5/3}},$$

Table 5
Estimation of u_{cr}^* using Eq. (9)

Q (kW)	T-profile	Q^*	u_{cr}^* Eq. (9)	u_{cr}^* CFD	$\Delta T_{cf}/\Delta T_{avg}$	$\Delta T_{cf}/T_{avg}$	$\tilde{H}(m)$
3	(a)A	0.039	0.392	0.268	0.928	0.078	0.343
53	(a)B	0.693	0.503	0.480	1.708	0.836	0.343
89	(a)C	1.170	0.506	0.482	1.146	0.776	0.343
13500	(b)A	0.073	0.310	0.325	3.47	0.400	7.07
67200	(b)B	0.366	0.444	0.406	1.906	0.745	7.07
143800	(b)C	0.783	0.475	0.406	1.257	0.771	7.07

where $\Delta\rho$ is the density difference above ambient. The buoyancy head Δp can then be estimated as

$$\Delta p_{\text{buoyancy}} = \int_0^H \Delta\rho g \, \mathrm{d}z \propto \frac{Q^{2/3}}{H^{2/3}} \tag{13}$$

For a very large fire with continuous flaming to roof level, the temperature is roughly constant above the fire and the density difference becomes a constant value $\Delta\rho_f$ for all z and Q. Figs. 14 and 15 show that this statement may not be true. The buoyancy head becomes

$$\Delta p_{\text{buoyancy}} = \int_0^H \Delta\rho_f g \, \mathrm{d}z \propto H \tag{14}$$

Oka and Atkinson [7] argued that, at the critical ventilation velocity, the ratio of the dynamic head of the inflow to the buoyancy head above the fire must exceed a critical value, or

$$\left[\frac{\Delta p_{\text{dynamic}}}{\Delta p_{\text{buoyancy}}}\right]_{cr} > C_{cr} \tag{15}$$

For small fires this becomes (using Eq. (13) and $\Delta p_{\text{dynamic}} = \rho_{in}(u_{cr}^2/2)$

$$u_{cr} > C_{cr}^{1/2}\left[\frac{Q}{H}\right]^{1/3} \tag{16}$$

This implied that u_{cr} is proportional to $Q^{1/3}$ for a small Q. For large fires we get, using Eq. (14),

$$u_{cr} > C_{cr}^{1/2} H^{1/2} \tag{17}$$

Thus, u_{cr} is independent of Q for a large Q.

4.8. Comparison with simple theories

Kennedy et al. [6] developed a theory for the critical ventilation velocity in a fire tunnel. The theory is based on an overall heat balance in one-dimensional flow of a fire tunnel, and is given by Eq. (12). It is noted that this set of equations in Q and u_{cr}

are non-linear. A FORTRAN program was written to obtain a set of Q and u_{cr} for the large tunnel.

By using a two-dimensional approach, Kunsch developed a model for the critical ventilation velocity in a ventilated tunnel [12]. The critical ventilation velocity is given by

$$u^*_{cr} = C_3\sqrt{C_1\Delta T^*_0}\frac{\sqrt{1+(1-C_2/C_1)\Delta T^*_0 Q^{*2/3}}}{1+\Delta T^*_0 Q^{*2/3}}\,Q^{*1/3} \tag{18}$$

with

$$C_1 = \frac{1-0.1(H/W)}{1+0.1(H/W)}\left[1+0.10\left(\frac{H}{W}\right)-0.015\left(\frac{H}{W}\right)^2\right] \cong 1-0.10\left(\frac{H}{W}\right),$$

$$C_2 = \frac{1-0.10(H/W)}{1+0.10(H/W)}0.574\left(1-0.20\frac{H}{W}\right),$$

$$C_3 = 0.613,$$

where ΔT^*_0 is a dimensionless constant with a value equal to 6.13, and W is the tunnel width in meter.

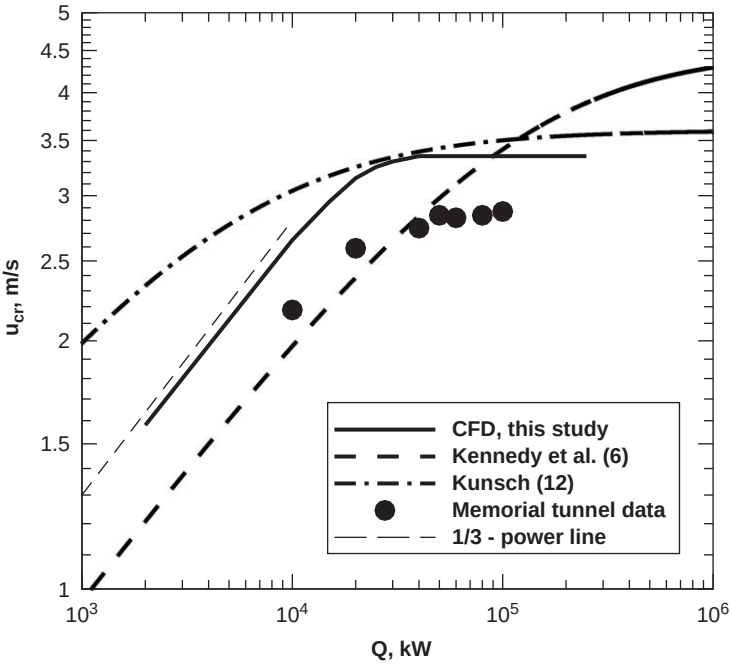

Fig. 17. Comparison of two simple theories with the results of the present CFD simulations for the large fire tunnel.

Fig. 17 shows the plots of Eqs. (12) and (18) with data that applied to the large tunnel. The CFD results are also shown for comparison. The lines representing these simple theories and the CFD results cross at $Q \approx 10^5$ kW. For Q below 10^5 kW, the CFD simulation predict the values of u_{cr} approximately the average of those predicted by these two theories. Although the simple theories predict leveling-off of u^*_{cr} as Q^* increases, CFD results give better agreement with the experimental trend. It is noted that the simple theories are based on analyses of one-dimensional or two-dimensional flows while the CFD results are based on three-dimensional tunnel flow. A simple theory does not include the complex flow patterns associated with the rising hot plume. Neither does it include the fire-source geometry or gas radiation. The present CFD results provide details of 3-D flow patterns with reasonable computer time.

5. Discussions and conclusions

In the present investigation, a CFD code FDS2 was employed to predict the critical ventilation velocity in fire tunnels. Tunnels of different sizes and fire-source geometries were selected for simulations. The following observations are made from the present study.

(1) When the critical ventilation velocity u_{in} is plotted against the fire heat generation rate Q as shown in Fig. 2, u_{cr} is roughly proportional to the 1/5 power of Q. This plot encompasses all available data of tunnel sizes. It is noted that there are subgroups of points for tunnels of different size. Each subgroup has its maximum u_{cr}, the critical velocity at leveling-off. For each tunnel size, if we take the points in Fig. 2 where u_{cr} begins to level off and connect these points with a straight line, the line has approximately 1/5th power. For example, for the Memorial tunnel the point is (3×10^4 MW, 2.9 m/s), and for the tunnel A, Wu and Bakar the point is (5 kW, 0.48 m/s). The straight line connecting these two points in Fig. 2 has approximately 1/5th power. According to Quintiere [31], the reference velocity V for a fire plume is

$$V = \sqrt{g}\left(\frac{Q}{\rho_0 \sqrt{g} c_p T_0}\right)^{1/5}$$

It can be argued that the fire-plume velocity is the base velocity of the back-layer velocity when the plume reaches the ceiling region. The back-layer velocity eventually becomes zero (or turns around) at $x = 0$ for critical ventilation. This process involves the ventilation velocity in contact with the back-layer. Therefore,

$$(u_{cr})_{max} \propto V \propto Q^{1/5}$$

where $(u_{cr})_{max}$ is the value of u_{cr} at leveling-off. In Fig. 3, the subgroup slides along the 1/5th power line when the scaling factor $\bar{H}$ is applied through the Froude Modeling. Within the subgroup, $u_{cr} \propto Q^{1/3}$ for small Q's.

(2) The CFD results clearly show the leveling-off of the critical ventilation velocity as the fire heat generation increases. Previous workers have established similar

trend experimentally. The leveling-off of the critical ventilation velocity can be explained by the temperature maximum above the fire source.

(3) The concept of temperature stratification in fire tunnel [14] is applied to the temperature profiles obtained by the present CFD simulations for both the small and the large tunnels. A new parameter for temperature stratification appears to be more consistent for the present application than the one defined by Newman [14].

(4) The CFD results show that the fuel type and the ambient temperature have negligible effects on the value of u_{cr}.

(5) The tunnel configuration (size and fire-source configuration) appears to have effects on the $u^*_{cr} - Q^*$ relationship. It may be noted that the Froude modeling used in the correlation requires geometric similarity. When such similarity is not maintained as in our small channel and large tunnels, a perfect Froude modeling cannot be expected. The results of the present simulations show that maintaining the geometrical similarity for tunnels cannot maintain the kinematical similarity. This indicates that the Froude-scaling law is an approximation for tunnel fires.

(6) In the simple theories using one- or two-dimensional approach, the leveling-off of the critical ventilation is also predicted, though not as sharply as the results shown in experiments and CFD. The parameter, layer width W, appears in the two-dimensional theory, and does not appear in the Froude modeling [12]. The introduction of the hydraulic tunnel height $\bar{H}$ effectively absorbs the parameter W [11]. As long as the channel cross-section does not deviate too far from a square, approximate geometrical similarity is maintained. Since the aspect ratio of the tunnels used in the practical application are not too large, an extrapolation of small-scale results is approximately valid.

(7) The FDS code using LES turbulence model [20] is capable of predicting the critical ventilation velocity in channels of various size and configuration. The effect of tunnel inclination on the critical ventilation velocity is also predicted. The results compare well with existing experimental data. Comparisons with the results of previous authors are also made. The agreement with these results and the present CFD results is fair. As expected, in an inclined tunnel with ascensional ventilation, a smaller ventilation velocity is required to prevent back layering of the hot gas than in a horizontal tunnel. The change in the ventilation velocity is a non-linear function of the inclined angle of the tunnel.

References

[1] Thomas PH. Movement of smoke in horizontal corridors against an air flow. Inst Fire Engrs Q 1970;30:45–53.

[2] Massachusetts Highway Department. Boston, MA: Memorial tunnel fire ventilation test program, Test Report, 1995.

[3] Hwang CC, Wargo JD. Experimental study of thermally generated reverse stratified layers in a fire tunnel. Combust Flame 1986;66:171–80.

[4] Heselden AJM. Studies of fire and smoke behavior relevant to tunnels. In: Proceedings of the second international symposium on the aerodynamics and ventilation of vehicle tunnels. Cambridge, UK: BHRA Fluid Engineering; 1976, pp. 23–5.

[5] Guelzim A, Souil JM, Vantelon JP, Sou DK, Gabay D, Dallest D. Modelling of a reverse layer of fire-induced smoke in a tunnel. Fire safety science proceeding of the fourth international symposium; 1994, pp. 277–88.
[6] Kennedy WD, Gonzales JA, Sanchez JG. Derivation and application of the SES critical velocity equations. ASHRAE Trans: Research 1996;102(2):40–4.
[7] Oka Y, Atkinson GT. Control of smoke flow in tunnel fires. Fire Safety J 1996;25:305–22.
[8] Hwang CC, Chaiken RF, Singer JM, Chi DNH. Reverse stratified flow in duct fires: a two-dimensional approach. In: 16th symposium international on combustion. Pittsburgh: The Combustion Institute; 1977, pp. 1385–95.
[9] Charters DA, Gray WA, McIntosh AC. A computer model to assess fire hazards in tunnels (FASIT). Fire Technol 1994;30:134–54.
[10] Grant GB, Jagger SF, Lea GJ. Fires in tunnels. Philos Trans R Soc London A 1998;356:2873–906.
[11] Wu Y, Bakar MZA. Control of smoke flow in tunnel fires using longitudinal ventilation systems—a study of the critical velocity. Fire Safety J 2000;35:363–90.
[12] Kunsch JP. Simple model for control of fire gases in a ventilated tunnel. Fire Safety J 2002;37:67–81.
[13] McCaffrey BJ, Quintiere JG. Buoyancy driven countercurrent flows generated by a fire source. In: Spalding DB, Afgan N, editors. Heat Transfer and Turbulent Buoyant Convection. Washington, USA: Hemisphere Publishing co.; 1977. p. 457–72.
[14] Newman JS. Experimental evaluation of fire-induced stratification. Combust Flame 1984;57:33–9.
[15] Hwang CC, Edwards JC. CFD Modeling of smoke reversal. In: Proceedings of the international conference on engineering fire protection design. Bethesda, Maryland, USA: Society of Fire Protection Engineers; 2001, pp. 376–87.
[16] McGrattan KB, Baum HR, Rehm RG, Hamins A, Forney GP, Floyd JE, Hostikka S. Fire dynamics simulator (version 2)—technical reference guide. NIST report no NISTIR 6783. Gaithersburg, Maryland: National Institute of Standards and Technology; 2001.
[17] Xue H, Hihara E, Saito T. Turbulence model of fire-induced air flow in a ventilated tunnel. Int. J. Heat Mass Transfer 1993;36:1739–48.
[18] Sinai YL, Owens MP. Validation of CFD modeling of unconfined pool fire with cross-wind: flame geometry. Fire Safety J 1995;24:1–34.
[19] Woodburn PJ, Britter RE. CFD simulations of a tunnel fire—Part I. Fire Safety J 1996;26:35–62.
[20] McGratten KB, Forney GP, Floyd JE, Hostikka S. Fire dynamics simulator ——user's guide (version 2). NIST report no NISTIR 6784. Gaithersburg, Maryland: National Institute of Standards and Technology, 2001.
[21] Givi P. Model-free simulations of turbulent reactive flows. Prog. Energy Combut. Sci. 1989;15:1–107.
[22] Smagorinsky J. General circulation experiments with the primitive equations. I. the basic experiment. Monthly Weather Rev 1963;91:99–164.
[23] Poinsot T, Veynante D. Theoretical and numerical combustion. Philadelphia, PA, USA: Edwards Inc.; 2001.
[24] Baum HR, McGrattan KB, Rehm RG. Simulation of smoke plumes from large pool fires. In: Proceedings of the 25th symposium (international) on combustion. Pittsburgh: The Combustion Institute; 1994, pp. 1463–69.
[25] Baum HR, Ezekoye OA, McGrattan KB, Rehm RG. Mathematical modeling and computer simulation of fire phenomena. Theor Comput Fluid Dynam 1994;6:125–39.
[26] Baum HR, McGrattan KB, Rehm RG. Three dimensional simulations of fire plume dynamics. J Heat Transfer Soc of Japan 1997;35:452–5.
[27] McGrattan KB, Baum HR, Rehm RG. Large eddy simulations of smoke movement. Fire Safety J 1998;30:161–78.
[28] Emmerich S, McGrattan KB. Application of large eddy simulation model to study room air flow. ASHRAE Trans 1998;104(1B):1128–40.
[29] Atkinson GT, Wu Y. Smoke control in sloping tunnels. Fire Safety J 1996;27:335–41.
[30] MaCaffery BJ. Purely buoyant diffusion flames: some experimental results. NBSIR 79-1910. Gaithersburg, Maryland, USA: National Bureau of Standards; 1979.
[31] Quintiere JG. Scaling applications in fire research. Fire Safety J 1989;15:3–29.